ROYAL SOCIETY
OF CHEMISTRY

Journal Name

ARTICLE

Experimental Study of Speciation and Mechanistic Implications when Using Chelating Ligands in Aryl–Alkynyl Stille Coupling[‡]

Ana M. Gallego, Marconi N. Peñas-Defrutos, Guillermo Marcos-Ayuso, Jose M. Martin-Alvarez, Jesús M. Martínez-Ilarduya, and Pablo Espinet*

Neutral palladium(II) complexes [Pd(Rf)X(P-L)] (Rf = 3,5-$C_6Cl_2F_3$, X = Cl, I, OTf) with P-P (dppe and dppf) and P-N (PPh$_2$(bzN)) ligands have chelated structures in the solid-state, except for P-L = dppf and X = Cl, were chelated and dimeric bridged structures are found. The species present in solution in different solvents (CDCl$_3$, THF, NMP and HMPA) have been characterised by ^{19}F and ^{31}P{^{1}H} NMR and conductivity studies. Some [Pd(Rf)X(P-L)] complexes are involved in equilibria with [Pd(Rf)(solv)(P-L)]X, depending on the solvent and X. The ΔH° and ΔS° values of these equilibria explain the variations of ionic vs. neutral complexes in the range 183-293 K. Overall the order of coordination strength of solvents and anionic ligands is: HMPA >> NMP > THF and I$^-$, Cl$^-$ > TfO$^-$. This coordination preference is determining the complexes participating in the alkynyl transmetalation from PhC≡CSnBu$_3$ to [Pd(Rf)X(P-L)] (X = OTf, I) in THF and subsequent coupling. Very different reaction rates and stability of intermediates are observed for similar complexes, revealing neglected complexities that catalytic cycles have to deal with. Rich information on the evolution of these Stille systems after transmetalation has been obtained that leads to proposal of a common behaviour for complexes with dppe and PPh$_2$(bzN), but a different evolution for the complexes with dppf: This difference leads the latter to produce PhC≡CRf and black Pd, whereas the two former yield PhC≡CRf and [Pd(C≡CPh)(SnBu$_3$)(dppe)] or [Pd(C≡CPh)(SnBu$_3$){PPh$_2$(bzN)}].

Introduction

Pd-catalysed cross-coupling reactions are a most powerful C–C and C–heteroatom bond-forming tool.[1,2] The catalysts used are either isolated complexes or complexes synthesized in situ from appropriate precursors. Often no further consideration on their exact nature in the flask is made. However, speciation of the catalysts in solution is very important because, as shown for instance in our studies on the Stille process,[3,4,5,6] it can be determining of the transmetalation mechanism (cyclic, open, or via solvent-coordinated cationic species) and can be critical for the outcome of the processes.[7] Some time ago we examined, in the context of Stille reactions, the speciation, due to equilibria represented in Eqn. (1), of [Pd(Pf)X(PPh$_3$)$_2$] (Pf = C$_6$F$_5$; X = Cl, Br, I, OTf) in THF, NMP (N-methyl-2-pyrrolidone), and HMPA (hexamethylphosphoramide). These are solvents with different coordinating ability, utilized in coupling reactions where the oxidative addition of PfX to Pd^0 species in the catalytic cycle gives rise to [Pd(Pf)XL$_2$].
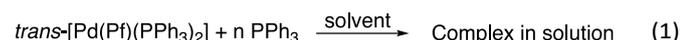
$$\text{trans-}[Pd(Pf)(PPh_3)_2] + n\ PPh_3 \xrightarrow{\ \text{solvent}\ } \text{Complex in solution} \quad (1)$$

Table 1 shows that, depending on X, n, and the solvent, several species can coexist, with features leading to different electrophilicity of the Pd centre, and opening alternative pathways to the next catalytic steps.

Table 1. Speciation of palladium PPh$_3$ complexes under different conditions

X	solvent	n	Complexes in solution
Cl,Br,I	THF	0	trans-[Pd(Pf)X(PPh$_3$)$_2$]
OTf	THF	0	trans-[Pd(Pf)X(PPh$_3$)$_2$] + [Pd(Pf)(solv)(PPh$_3$)$_2$]X in equilibrium
I	NMP	0	trans-[Pd(Pf)X(PPh$_3$)$_2$]
OTf	NMP	0, 2	trans-[Pd(Pf)(solv)(PPh$_3$)$_2$]X
Cl	HMPA	0	trans-[Pd(Pf)(solv)(PPh$_3$)$_2$]X 62% + cis-[Pd(Pf)(solv)$_2$(PPh$_3$)]X 18% + trans(Cl-Pf)-[Pd(Pf)X(solv)(PPh$_3$)] 20%
Cl,Br,OTf	HMPA	2	trans-[Pd(Pf)(solv)(PPh$_3$)$_2$]X

Chelating ligands look, in principle, ideal to favour a cis coordination of the two groups to be cross-coupled, which is a requirement for coupling, but in practice, they have also shown to have disadvantages. For instance, in the study of the coupling of PfOTf and CH$_2$=CHSnBu$_3$ catalyzed by [Pd(Pf)(OTf)(dppe)], our group observed the key intermediates of the catalytic cycle, including the transmetalation product [Pd(Pf)(CH=CH$_2$)(dppe)],[8] but the reductive elimination step at room temperature was

very slow because of the strongly chelating dppe. In fact, complexes carrying too strong chelating ligands frequently do not lead to good results in catalysis,[9] but many exceptions are also known, not only in Pd-catalysed reactions,[10] but also in cooperative Cu/Pd catalysed reactions, *e.g.* the recently reported for allylboration of alkynes using dppf as Pd ligand.[11]

An interesting case of Stille catalysis is the Pd-catalysed aryl–alkynyl cross coupling using alkynyl stannane, where the behaviour of monodentate and chelating ligands drastically differs in an unexpected direction: the monodentate phosphine PPh$_3$ is very inefficient, but some (nor any) diphosphines or P-N ligands make the process very efficient.[12,13] A thorough mechanistic study of the PPh$_3$ case uncovered a many-pathways reaction and revealed that the reason for the partial frustration of PhC≡C–Rf coupling (Rf = 3,5-C$_6$Cl$_2$F$_3$) is the formation of *trans*-[Pd(Rf)(C≡CPh)(PPh$_3$)$_2$], which is reluctant to isomerize to cis as required for coupling.[14] The good results with some chelating ligands suggest that they will enforce the required cis configuration. However, there have not been any detailed mechanistic studies of this process.[15]

In this paper we report the synthesis, structural study and speciation in three different solvents (THF, NMP, and HMPA) of [Pd(Rf)X(P-L)] complexes (X = halide or triflate) for the chelating ligands shown in Fig. 1, which include two frequently used chelating diphosphines and one potentially hemilabile P-N ligand. The speciation data help to understand the mechanism of transmetalation, a step common to the different Pd cross-coupling catalytic cycles that is studied here for the Stille coupling between [Pd(Rf)X(P-L)] (X = OTf, I) and PhC≡CSnBu$_3$. The aryl Rf provides stability to the aryl complexes, allows us to obtain single crystals, and enables meaningful ^{19}F NMR studies. All the experimental information is detailed in the ESI.


Fig. 1. P-L ligands used in this work.

Results and discussion

1. Synthesis and characterization in the solid state and in CDCl$_3$ solution of [Pd(Rf)X(P-L)] (X = Cl, I, OTf) complexes.

The synthesis of the Rf palladium complexes with the ligands depicted in Fig. 1 is summarised in Scheme 1. Reacting (2:1) the corresponding P-L ligand with (μ-Cl)$_2$[Pd(Rf)(tht)]$_2$ (**1**) (tht = tetrahydrothiophene)[16] affords [Pd(Rf)Cl(P-L)] (P-L = dppe, **2a**; dppf, **2b**; PPh$_2$(bzN), **2c**) in high yield. For dppe and PPh$_2$(bzN) the reactions are as shown in the Scheme 1. However, in the reaction of **1** with dppf a small amount of a yellow solid precipitates, while most of the product remains in solution. The structures of the two competitively formed complexes were solved, and revealed two structural isomers.
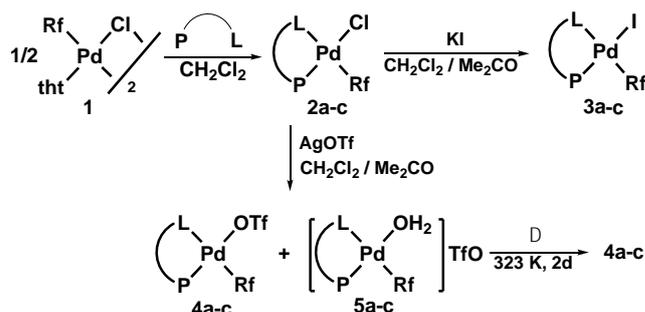
**Scheme 1.** Synthesis of the complexes used in this work. Rf = 3,5-C$_6$Cl$_2$F$_3$
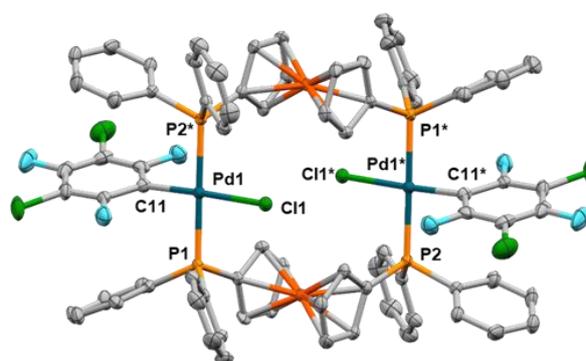
Fig. 2. Molecular structure of (μ-dppf)$_2$[Pd(Rf)Cl]$_2$ (**2b-dim**). All hydrogen atoms, as well as solvent molecules, have been omitted for clarity. Selected bond lengths (Å) and angles (°): Pd(1)–Cl(1) = 2.334(2), Pd(1)–P(2*) = 2.3170(19), Pd(1)–P(1) = 2.361(2), Pd(1)–C(11) = 2.015(8).

The major and most soluble isomer is a monomer (Fig. ESI 1), [Pd(Rf)Cl(dppf)] (**2b**), that displays *cis*-P-P coordination to Pd with a P–Pd–P bite angle 100.55(3)°, slightly larger than the average bite angle value reported for this diphosphine (99°).[17] The less soluble isomer (Fig. 2) is dimeric, **2b-dim**, and displays two bridging dppf ligands, mutually trans and monodentate at each palladium.[18]

Halide metatheses of [Pd(Rf)Cl(P-L)] (**2a-2c**) with KI (excess) in acetone/dichloromethane (v/v = 1:1) afford the iodo complexes [Pd(Rf)I(P-L)] with P-L = dppe (**3a**), dppf (**3b**), or PPh$_2$(bzN) (**3c**), as shown in Scheme 1. The X-ray structure of **3c** (Fig. ESI 2) confirms that the two strong soft ligands (Rf and P) choose cis positions (antisymbiotic behaviour).[19]

In the reactions with AgOTf, the presence of adventitious water in the solvents, produced mixtures in solution of the triflate complexes [Pd(Rf)(OTf)(P-L)] (**4a-4c**) and [Pd(Rf)(OH$_2$)(P-L)](TfO) (**5a-5c**), also present in the solid state. These structures are supported in all cases by C,H,N analysis, ^{19}F, ^{31}P and ^{1}H NMR spectra, and IR data: a broad band close to 3270 cm^{-1} is due to the ν(O–H) stretching absorptions of coordinated water, and bands due to free (1300 cm^{-1}) and coordinated triflate (1230, 1210, and 1190 cm^{-1}) are also observed. Heating the mixtures up to constant weight (about 2-3 days) in an oven at 50 °C led to complete elimination of H$_2$O, giving pure [Pd(Rf)(OTf)(P-L)] complexes.

The X-ray structure of **5c** (Fig. 3) shows bonds lengths and angles typical for other complexes containing the PPh$_2$(bzN) ligand. The water ligand is involved in hydrogen bonding to the triflate anions, giving rise to dimers in the crystal (Fig. ESI 3).
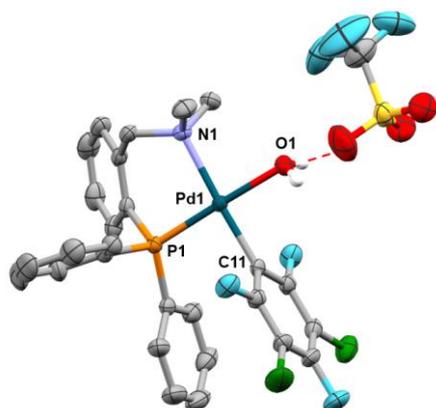

Fig. 3. Molecular structure of **5c**. Most hydrogen atoms, as well as solvent molecules, have been omitted for clarity. Selected bond lengths (Å) and bond angles (°): Pd(1)–P(1) = 2.2156(8), Pd(1)–N(1) = 2.162(3), Pd(1)–O(1) = 2.133(3), Pd(1)–C(11) = 2.008(3), N(1)–Pd(1)–P(1) = 93.31(7).

In the non-coordinating solvent CDCl$_3$ the neutral complexes (**2a-c**, **3a-c**, **4a-c**) do not dissociate into cationic species and their NMR spectra are consistent with the structures proposed in Scheme 1. In significant presence of adventitious water, OH$_2$ competes with the triflate anion for the coordination position, and equilibria **4a-c/5a-c** are established. The ^{31}P{^{1}H} spectra of the diphosphine complexes show two multiplets (1:1 ratio) due to P-P and P-F^o (*ortho*-fluorine) couplings. The upfield signal corresponds to the P atom trans to Rf, more shielded due to the high trans influence of this group. For the PPh$_2$(bzN) ligand, a triplet is observed in the ^{31}P{^{1}H} spectra, due to coupling to the two F^o atoms of the fluoroaryl group in cis (compound **4c**), or a triplet of doublets when the resolution is able to detect also coupling to F^p (compounds **2c** and **3c**). All the NMR information is given in ESI.

In none of the structures studied is the Pd coordination plane a symmetry plane. Since perhaloaryl groups in Pd square-planar complexes have high rotational barriers,[20] chemical non-equivalence of the two F^o atoms should be expected. However, the ^{19}F NMR spectra at 298 K of the reported complexes show chemical equivalence, except for the PPh$_2$(bzN) complexes where broad signals are observed. Lower temperatures lead to different degrees of broadening in the other complexes. This suggests that the chemical equivalence observed at 298 K is attained by fast conformational inversion of the non-planar palladacycles formed upon P-L coordination,[21] which are plane-averaged in the NMR time scale at temperatures depending on the complex.

2. Equilibria between [Pd(Rf)X(P-L)] (X = Cl, I, OTf) and [Pd(Rf)(solv)(P-L)]X complexes in THF, NMP and HMPA.

The behaviour of the neutral complexes [Pd(Rf)X(P-L)] (X = Cl, I, OTf) in THF, NMP, and HMPA is reported below. The NMR spectra of the halo complexes [Pd(Rf)X(P-L)] (X = Cl, I) in THF,

are similar to those obtained in CDCl$_3$. However the ^{19}F NMR of the triflate complexes **4b** and **4c** (not **4a**) indicate the existence of entropy dependent equilibria of the neutral complexes with [Pd(Rf)(THF)(P-L)](OTf) (P-L = dppf, **6b**; PPh$_2$(bzN), **6c**), which show strong temperature dependence (see Fig. 4 for **4b/6b**). Participation of some adventitious water in these complexes, in fast THF/OH$_2$ exchange, is highly probable.
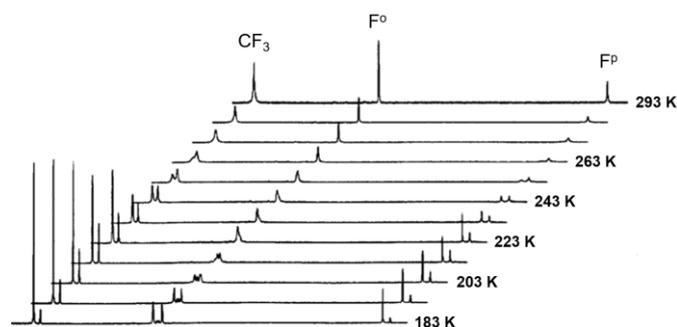

Fig. 4. Variable temperature ^{19}F NMR of a solution of [Pd(Rf)(OTf)(dppf)] (**4b**) in dry THF as solvent.

The CF$_3$ signal of OTf, and the F^p signals of Rf allow us to observe **4b** and **6b** separately at low temperatures (Fig. 4). We detect OTf/THF exchange and inversion of the **4b/6b** relative abundance in solution at higher temperatures (above 243 K). For unambiguous assignment of the **4b** and **6b** signals, the cationic complex [Pd(Rf)(THF)(dppf)](BF$_4$) (**6b***), with a non-coordinating anion, was synthesized in situ at 183 K treating **2b** with AgBF$_4$ in dry THF. This reference complex proves that, for triflate, the ionic complex is the one very predominant at low temperature, but its percentage in the mixture diminishes as the temperature increases. In addition, above 243 K all the signals start to show broadening as symptom of slow neutral/cationic exchange. At 293 K they appear as thin averaged signals above coalescence, corresponding to a fast equilibrium exchange. Plotting –lnK *vs* 1/T in the low temperature range (183–243 K), the thermodynamic parameters for the neutral/cationic equilibrium were calculated: ΔH° = –18.4±0.9 kJ mol^{-1}; ΔS° = –77±4 J K^{-1} mol^{-1}. The small value of ΔH° makes the equilibrium highly entropy and temperature dependent, as observed.[22] With these data in hand, the equilibrium constant and the neutral/ionic complex ratio in THF at any temperature can be calculated. In a catalytic process this ratio could be relevant in order to determine the preferred catalytic mechanism. In the case of dppf, the Pd ratio **4b/6b** is 92/8 (K$_{323}$ = 0.085) for a solution 10^{-2} M in Pd at 323 K. The same calculations for PPh$_2$(bzN) affords **4c/6c** = 96/4 molar ratio (K$_{323}$ = 0.043).

For **4a** in THF, only one species is observed at all temperatures tested. This unexpected result prompted us to perform conductivity measurements. The conductivity of [Pd(Rf)Cl(dppe)] (**2a**) was also measured for comparison (Table 2, entries 1-6). The molar conductivities for **4a** and **4b-c** are similar and much lower than for a 1:1 electrolyte (entry 1), suggesting the existence of similar neutral/ionic equilibria in the three cases. Hence, we suggest that the different NMR

behaviour of **4a** must be simply due to faster equilibration in solution.

As for the speciation of [Pd(Rf)X(P-L)] (X = Cl, I, OTf) in NMP and HMPA, these solvents are more strongly coordinating than THF, so it can be assumed safely that their triflate ligands in these solvents will be 100% in the ionic form, with at least one solvent molecule coordinated: [Pd(Rf)(solv)(P-L)](TfO) (solv = NMP (**7a-c**), HMPA (**8a-c**)). In fact, the ^{19}F NMR spectra confirm that NMP and HMPA are able to displace quantitatively the triflate at any temperature. These two solvents differ in that NMP is not able to displace extensively any halide from the metal coordination sphere, whereas the more strongly coordinating HMPA is able to displace the chloride ligand completely, and the iodide in a large extension in all the [Pd(Rf)X(P-L)] complexes (complete for P-L = PPh$_2$(bzN)). The equilibrium constants, measured by ^{19}F NMR in HMPA at 323 K with [Pd] = 10^{-2} M, are 0.057 (**3a**) and 0.106 (**3b**), corresponding to the neutral-complex/ionic-complex ratios 13/87 and 8/92, respectively.

All these observations were confirmed by the spectra obtained in separate experiments where quantitative formation of [Pd(Rf)(solv)(P-L)]$^+$ was forced upon addition of AgBF$_4$. The differences observed between the halo complexes (X = Cl *vs* I) must be attributed to an important contribution of the solvation energy of the anions ($E_{solv}Cl^- > E_{solv}I^-$), overcoming the behaviour expected from Pd–X bond energies (Pd–Cl > Pd–I). The molar conductivities in NMP and HMPA (Table 2, entries 7-17) are in good agreement with the previous results, supporting substantial displacement of I^- from palladium only in HMPA. This should open to halides ionic pathway in this solvent, as it happens for triflates in THF. Some moderate iodide displacement seems to occur in NMP, where a neutral/ionic equilibrium could exist to a small extent.[23]

Table 2. Molar conductivities (Λ_M) in THF, NMP and HMPA solutions at 298 K. (**rn** or **ri** stand for reference of neutral or ionic 1:1 electrolytes, respectively).

Entry	Solvent	Complex	Λ_M (S·cm^2·mol^{-1})
1(**ri**)	THF	[Pd(Rf)(PPh$_3$)(dppf)](TfO)	19
2	THF	[Pd(Rf)(OTf)(dppe)] (**4a**)	4
3	THF	[Pd(Rf)(OTf)(dppf)] (**4b**)	4
4	THF	[Pd(Rf)(OTf){Ph$_2$(bzN)}] (**4c**)	4
5	THF	[Pd(Rf)I(dppe)] (**3a**)	0
6(**rn**)	THF	[Pd(Rf)Cl(dppe)] (**2a**)	0
7(**ri**)	NMP	[Pd(Rf)(PPh$_3$)(dppe)](TfO)	19
8	NMP	[Pd(Rf)(OTf)(dppe)] (**4a**)	17
9	NMP	[Pd(Rf)I(dppe)] (**3a**)	1
10	NMP	[Pd(Rf)I(dppf)] (**3b**)	2
11	NMP	[Pd(Rf)I{PPh$_2$(bzN)}] (**3c**)	2
12(**rn**)	NMP	[Pd(Rf)$_2$(dppe)]	0
13(**ri**)	HMPA	[Pd(Rf)(PPh$_3$)(dppe)](TfO)	14
14	HMPA	[Pd(Rf)I(dppe)] (**3a**)	15
15	HMPA	[Pd(Rf)I(dppf)] (**3b**)	14
16	HMPA	[Pd(Rf)I{PPh$_2$(bzN)}] (**3c**)	15
17(**rn**)	HMPA	[Pd(Rf)$_2$(dppe)]	0

One could wonder whether these stronger solvents might displace the N extreme of the ligand PPh$_2$(bzN) from palladium, but the observation of two (1:1) non-equivalent F_{ortho} signals in both solvents suggests that this does not occur.[24] A summary of the results of this speciation study is given in Table 3.

Table 3. Summary of the speciation observed in different solvents for the complexes studied in this work. N = [Pd(Rf)X(P-L)]; CAT = [Pd(Rf)(solv)(P-L)]$^+$X$^-$.

X	CDCl$_3$	THF	NMP	HMPA
Cl	N	N	N	CAT
I	N	N	N	N + CAT*
OTf	N + CAT(OH$_2$)	N + CAT	CAT	CAT

* Only the cationic species is observed for X = I and P-L = PPh$_2$(bzN)

3. Kinetic monitoring of transmetalation reactions in THF using excess PhC≡CSnBu$_3$ and [Pd(Rf)X(P-L)] (X = OTf, I).

The reactions of [Pd(Rf)X(P-L)] with an excess of PhC≡CSnBu$_3$ (**9**) were monitored in THF by ^{19}F NMR (Eqn. 2) for: *i)* X = TfO, as an example of anion either ionized in THF (Table 3) or expected to be easily substituted by the triple bond of the reagent (hence expected to follow an ionic transmetalation pathway); *ii)* and for X = I as an example of coordinated anion reluctant to facilitate ionization in THF. The absence of RfI or RfOTf precludes the classical oxidative addition leading, in the catalytic processes, to further evolution.[25]

$$\binom{L}{P}Pd\binom{X}{Rf} + 20\ Ph\!\!=\!\!=\!\!SnBu_3 \xrightarrow{THF} Ph\!\!=\!\!=\!\!Rf \qquad (2)$$
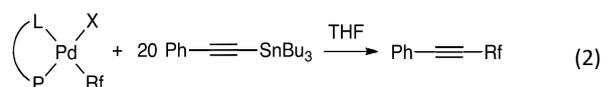
A Pd:Sn = 1:20 ratio was used in order to reproduce a frequent catalytic proportion. Note that the products lacking Rf do not show in the ^{19}F NMR monitoring, but can be followed by ^{31}P NMR. The results of these studies led to the general pathways in Scheme 2.
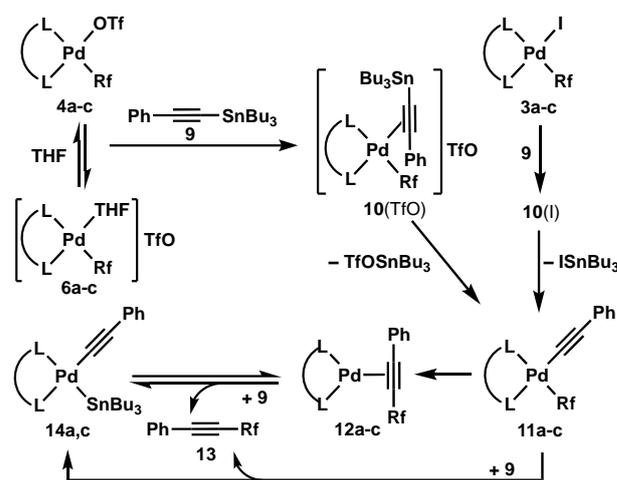
Scheme 2. Products detected in the reactions of [Pd(Rf)X(P-L)] (X = OTf, **4a-c**; X = I, **3a-c**) with an excess of PhC≡CSnBu$_3$ (**9**) (Pd:Sn = 1:20) in THF.

3.1.a. Transmetalation to [Pd(Rf)(OTf)(dppe)] (4a) in THF.

When [Pd(Rf)(OTf)(dppe)] (**4a**) and PhC≡CSnBu$_3$ (**9**) were mixed in THF at 313 K, a fast transmetalation (instantaneous for the standards

of the monitoring) took place giving [Pd(Rf)(C≡CPh)(dppe)] (**11a**), which started to evolve *slowly* to the initial reduction product [Pd(η²-PhC≡CRf)(dppe)] (**12a**), and the coupling product PhC≡CRf (**13**), as plotted in Fig. 5. For a long time, *no black Pd is observed* because, as shown in Scheme 2, the formation of **13** is concomitant with the participation of a second molecule of the alkynylstannane **9**, yielding **14a** (observed by $^{31}P\{^1H\}$ NMR). Only at very long times black Pd is formed by slow decomposition. The experimental evolution was perfectly fitted (continuous lines) with COPASI software,[26] applying the equations in Scheme 3 (full details in ESI). The adjusted rate constants for the competitive evolution from **11a** yield very precise values: $(2.63\pm0.07) \times 10^{-5}$ s^{-1} for k_3, and $(1.26\pm0.03) \times 10^{-4}$ mol^{-1} L s^{-1} for k_4 .
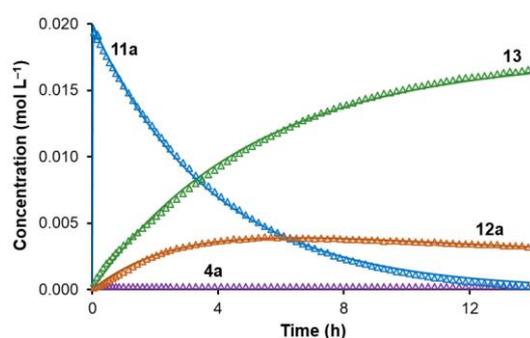
**Fig. 5.** ^{19}F NMR monitoring of the reaction of [Pd(Rf)(OTf)(dppe)] (**4a**) with PhC≡CSnBu₃ (**9**) (Pd:Sn = 1:20) at 313 K. Continuous lines are the result of COPASI fitting.
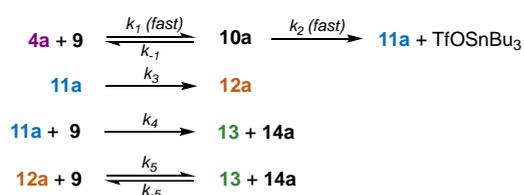
Scheme 3. COPASI equations for the kinetic simulations of the reaction of [Pd(Rf)(OTf)(dppe)] (**4a**) with an excess of PhC≡CSnBu₃ (**9**) (Pd:Sn = 1:20) in THF.

The same reaction was studied starting at 220 K, which allowed us to observe and identify an initial intermediate species [Pd(Rf)(η²-PhC≡CSnBu₃)(dppe)](TfO), **10a**(TfO), formed by substitution of TfO⁻ or THF by PhC≡CSnBu₃ (**9**), in the equilibrium **4a/6a**.[27,28] The computed thermodynamics of ligand substitution in **6a⁺** of THF by **9**, in order to form **10a⁺**, is favourable by $\Delta G = -6.5$ kcal mol^{-1}. The proposed complex **10a**(TfO) could not be isolated, but the DFT optimised structure (wB97X-D level) of its cation **10a⁺** (with Me₃Sn instead of Bu₃Sn) is shown in Fig. 6. Interestingly, the coordination square plane of Pd is well defined by the two P atoms, the Rf group, and C1 of the alkyne, all at reasonable bond distances, but C2 is at long distance from Pd (2.557 Å). Moreover, whereas the C1–C2 distance is consistent with a triple bond, and the C1–C2–C$_{ipso}$ fragment is quite linear (176.48°), a remarkable bending is observed for Sn–C1–C2 (142.29°). These structural parameters are far from typical η²-alkyne coordination and point out to much higher implication of C1 than C2 electron density in this asymmetric coordination. Natural Bonding Orbital (NBO) and Second Order

Perturbation (SOPT) analyses, on optimised geometry of **10a⁺** support this hypothesis.
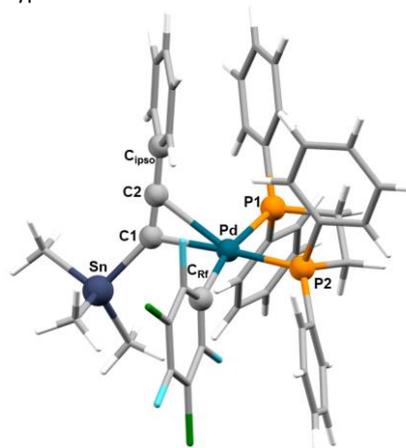

Fig. 6. DFT optimised structure of the cation **10a⁺**. Relevant distances (Å): Pd–C1 = 2.269; Pd–C2 = 2.557; C1–C2 = 1.237; Pd–P1 = 2.374; Pd–P2 = 2.290. Relevant angles (°): Sn–C1–C2 = 142.29; C1–C2–C$_{ipso}$ = 176.48.

Table 4. Selected Donor-Acceptor interactions and SOPT energies (kcal mol^1) for **10a⁺**.

Donor / Contribution	Acceptor / Contribution	E$_{SOPT}$
BD(3) C1–C2	**BD*(1) Pd–P2**	47.5
57% C1; p(100%)	71% Pd; s(48%) d(52%)	
43% C2; p(100%)	29% P2; s(28%) p(72%)	
BD(1) C1–Sn	**BD*(1) Pd–P2**	23.0
83% C1; s(55%) p(45%)	71% Pd; s(48%) d(52%)	
17% Sn; s(16%) p(84%)	29% P2; s(28%) p(72%)	

The atom labels are as in Fig. 6. BD and BD* stand, respectively, for bonding and antibonding orbitals.

Table 4 collects the two main donations from the alkyne moiety to palladium. The acceptor orbital is common for both interactions: the antibonding **BD*(1) Pd–P2** with high palladium contribution (*sd* electron density). The donors are different. One contains π-electron density of the triple bond (**BD(3) C1–C2**, 100% *p*) and accounts for the stronger donation. The other is a full bonding orbital **BD(1) C1–Sn**. The two have in common that they are polarised towards the C1 atom (57% and 83% respectively), which leads to an alkyne coordination much closer to η¹ than to η², very prone to the formation of the σ Pd–C1 bond found in **11a**, once the alkynyl transmetalation has been completed.

It is worth commenting that the steric crowding between the Rf ring and the PPh₂ group should impose severe restrictions to rotation around the Pd–Rf bond, and the alkynyl coordination perpendicular to the Pd coordination plane should give rise to chemical non-equivalence of the two F^o. Since this non-equivalence is not observed in the ^{19}F NMR spectra, equivalence must be achieved by fast rotation of the alkyne around the Pd-C1, confirming the proposed lesser implication of C2 in this alkyne coordination.

Already at the low temperature of 220 K, the alkynyl transmetalation is taking place slowly, leading to the σ-alkynyl complex [Pd(Rf)(C≡CPh)(dppe)] (**11a**). This transmetalation sequence reminds that of vinyl stannane, which also starts by coordination of the double bond of the vinyl group.[29] Complex **11a** was unambiguously characterised by NMR methods: its ^{19}F NMR spectrum shows the

resonances and chemical shifts expected for a Rf–Pd[II] group, with the F[o] coupled to the trans ($^4J_{\text{P-F}}$ = 12.6 Hz) and cis ($^4J_{\text{P-F}}$ = 3.3 Hz) ^{31}P atoms. In the ^{31}P{^{1}H} spectrum two signals at δ = 50.4 ppm (P trans to Rf) and δ = 55.2 ppm (P cis to Rf) are observed with $^2J_{\text{PP}}$ = 20.6 Hz. The molecular structure of **11a** could be solved (Fig. 7).
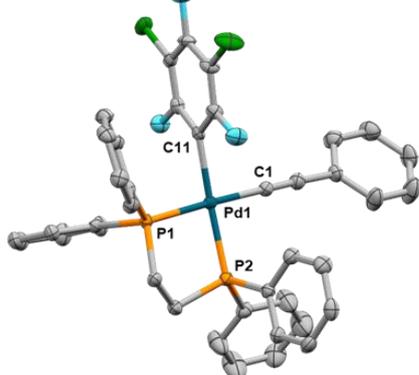

Fig. 7. Molecular structure of **11a**. All hydrogen atoms, as well as solvent molecules, have been omitted for clarity. Only one of the two slightly different molecules of the asymmetric unit is showed. Selected bond lengths (Å) and bond angles (°): Pd(1)–C(11) = 2.078(5); Pd(1)–P(1) = 2.2882(14); Pd(1)–P(2) = 2.2804(15); Pd(1)–C(1) = 2.019(6); P(1)–Pd(1)–P(2) = 85.84(5); C(1)–Pd(1)–P(2) = 96.76 (16); C(1)–Pd(1)–C(11) = 89.6(2); P(1)–Pd(1)–C(11) = 93.87(13).

At 263 K, complex **11a** starts to undergo reductive elimination and, in the presence of alkynyl stannane **9**, [Pd[0](η²-PhC≡CRf)(dppe)] (**12a**) and [Pd[II](C≡CPh)(SnBu₃)(dppe)] (**14a**) are formed, with concomitant release of PhC≡CRf (**13**). The ^{31}P{^{1}H} spectrum of **12a** shows an AB spin system consistent with a trigonal-planar coordinated Pd[0], with the triple bond of the asymmetric alkyne lying in the P–Pd–P plane. At higher temperature (295 K) more **13** is slowly released with increase of **14a**, which explains why only little black Pd is hardly observed. At higher temperatures (see Fig. 5 for the full evolution at 313 K), slow formation of more black Pd is observed with time.

In order to help with structural assessment of the Pd–Sn bonded species from the NMR signals in the reaction mixture, **14a** was independently prepared from [Pd(dba)(dppe)][30] (**15a**) and PhC≡CSnBu₃ (**9**).[31] The resulting ^{31}P{^{1}H} NMR spectrum of the latter reaction is shown in Fig. 8.
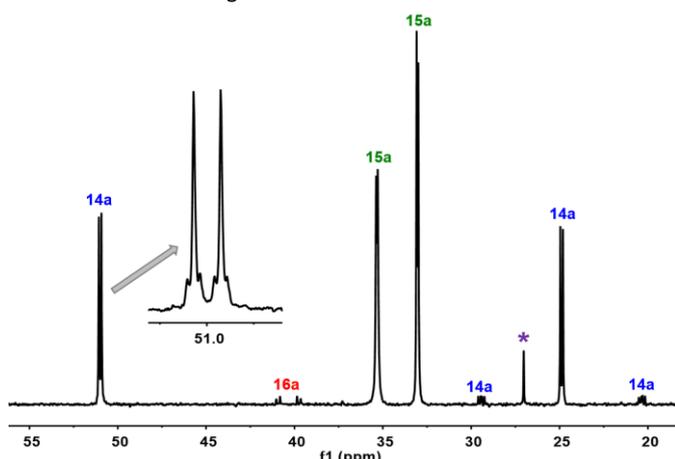
Fig. 8. ^{31}P{^{1}H} NMR spectrum of the reaction between [Pd(dba)(dppe)] (**15a**) and PhC≡CSnBu₃ (**9**) (Pd:Sn = 1:1), in THF, at 298 K.

It displays for **14a** two doublets (blue numbers) at 24.9 and 51.0 ppm ($^2J_{\text{PP}}$ = 24.5 Hz). The tin satellites ($^2J_{\text{P}^{117}\text{Sn}}$ = 1437 Hz and $^2J_{\text{P}^{119}\text{Sn}}$ = 1506

Hz) support that the upfield signal corresponds to the phosphorous atom trans to the stannyl group. In addition, the byproduct complexes [Pd(η²-PhC≡C–C≡CPh)(dppe)] (**16a**, red numbers),[32] [Pd(dppe)₂] (purple asterisk),[33] and unreacted **15a** (green numbers) are observed. The unusual oxidative addition of **9** to Pd[0] giving rise to **14a** was already reported by Shirakawa and Hiyama.[12,13]

Luckily, single crystals of the Pd–Sn bonded species **14a** could be obtained from the reaction mixture. Its molecular structure is shown in Fig. 9. Some structural aspects deserve comment: *i*) the complex displays clearly a Sn–Pd with intermetallic distance well below the sum of covalent radii (2.78 Å);[34] *ii*) The substantial elongation of the Pd(1)–P(1) distance, almost 0.1 Å longer than Pd(1)–P(2), proves the large *trans influence* of metal donors in a M–M' bond;[35] *iii*) The small C(1)–Pd(1)–Sn(1) (78.2°) and large P(2)–Pd(1)–Sn(1) (99.3°) angles may be related to steric hindrance issues provoked by the bulky SnBu₃ group.
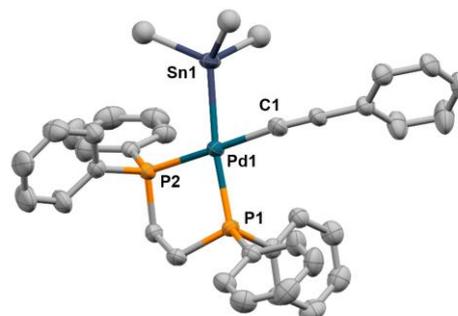

Fig. 9. Molecular structure of **14a**. All hydrogen atoms have been omitted and Bu groups have been also simplified for clarity. Selected bond lengths (Å) and bond angles (°): Pd(1)–Sn(1) = 2.5916(9); Pd(1)–C(1) = 2.009(10); Pd(1)–P(1) = 2.362(2); Pd(1)–P(2) = 2.271(2); P(1)–Pd(1)–P(2) = 85.99(8); C(1)–Pd(1)–Sn(1) = 78.2(3); C(1)–Pd(1)–P(1) = 96.1(3); Sn(1)–Pd(1)–P(2) = 99.31(7).

3.1.b. Transmetalation to [Pd(Rf)I(dppe)] (3a) in THF.

The kinetic profile of the reaction of [Pd(Rf)I(dppe)] (**3a**) and PhC≡CSnBu₃ (**9**), in THF at 313 K, is shown in Fig. 10 and reflects clearly that this transmetalation is considerably slower than for the triflato complex **4a**. In the case of **3a**, about 30% of the initial complex is still unreacted after 16 h at 313 K. Initially complex [Pd(Rf)(C≡CPh)(dppe)] (**11a**) is the product that is faster formed but its concentration starts to diminish relatively early in favour of [Pd(η²-PhC≡CRf)(dppe)] (**12a**) and PhC≡CRf (**13**) as the major products. In addition, [Pd(C≡CPh)(SnBu₃)(dppe)] (**14a**) is also formed as evidenced by ^{31}P{^{1}H} NMR spectra.
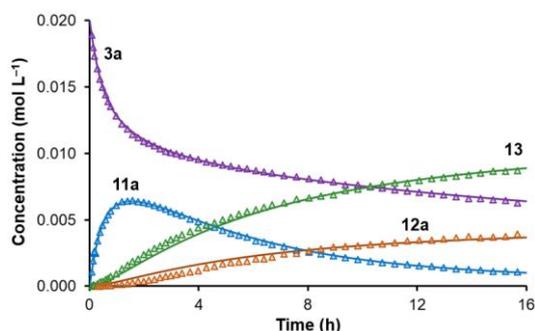
Fig. 10. ^{19}F NMR monitoring of the reaction between [Pd(Rf)I(dppe)] (**3a**) and PhC≡CSnBu₃ (**9**) (Pd:Sn = 1:20) in THF at 313 K. Continuous lines represent the kinetic fitting of data using COPASI software.

The abnormal consumption profile of the initial complex **3a**, which slows down not following a pseudo first order on Pd (**9** is in large excess), can be perfectly fitted (see Scheme 4 for the kinetic model, and Table ESI 5 for all numeric data). Clearly, the OTf⁻ for **9** or I⁻ for **9** ligand substitution equilibria are determinant of the transmetalation rate, since k_2 to complete the transmetalation is fast. In the COPASI equations the consumption of a second molecule of **9** per Pd, and the inhibition introduced by product **13** competing with **9** for I⁻ displacement, produce much more effect than in the reaction with triflate. This effect is detrimental for the formation of intermediate **10a**(I) (Scheme 2), and consequently slows down the transmetalation. We confirmed experimentally that the initial reaction rate falls dramatically in presence of added **13**. It is worth noting that the adjusted kinetic parameters for the evolution of the system from **11a** give values $(2.11\pm0.02) \times 10^{-5}$ s⁻¹ for k_3 and $(1.29\pm0.02) \times 10^{-4}$ mol⁻¹ L s⁻¹ for k_4, very similar to the ones obtained in the previous fitting with the OTf analogue (Fig. 5, Scheme 3).
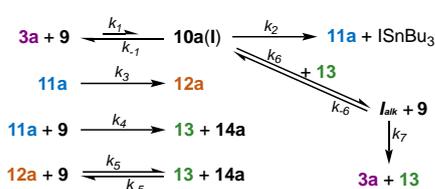
Scheme 4. Kinetic model for the reaction of [Pd(Rf)I(dppe)] (**3a**) with an excess of PhC≡CSnBu₃ (**9**). The inhibition of the conversion of **3a** by **13** is proposed to occur via [Pd(Rf)(η²-PhC≡CRf)(dppe)]I (**I_alk**), which is experimentally unobservable.

3.2.a. Transmetalation to [Pd(Rf)(OTf)(dppf)] (4b) in THF.

The reaction of [Pd(Rf)(OTf)(dppf)] (**4b**) with PhC≡CSnBu₃ (**9**) in THF at 313 K *is much faster* than with dppe and leads immediately to the coupling product PhC≡CRf (**13**) *and abundant black Pd*. Monitoring the reaction at 295 K, to make the different steps slower, we could observe some intermediates (Fig. 11).
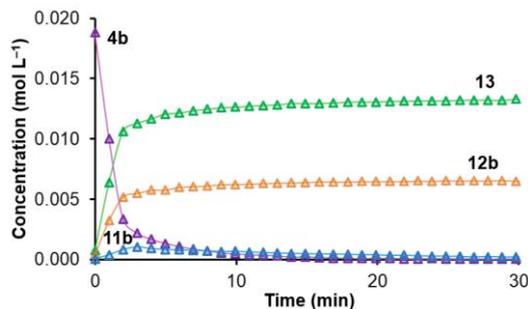
Fig. 11. ¹⁹F NMR monitoring of the reaction between [Pd(Rf)(OTf)(dppf)] (**4b**) and PhC≡CSnBu₃ (**9**) (Pd:Sn = 1:20) in THF at 295 K. In this case continuous lines are just to help the eye.

Although this fast process allowed only for acquisition of a lower number of data during monitoring, the profile confirms basically the same sequence of steps found for dppe in Scheme 2. At 220 K, intermediate [Pd(Rf)(η²-PhC≡CSnBu₃)(dppf)](TfO) (**10b**(TfO)) can be observed. Complex [Pd(Rf)(C≡CPh)(dppf)] (**11b**) is also observed, but [Pd(C≡CPh)(SnBu₃)(dppf)] (**14b**) s not detected. Overall the data indicate that the main qualitative difference occurs once **11b** has been formed. At variance with dppe, dppf is a wide bite angle ligand,[17] and efficiently induces cross coupling from **11b** to **12b**. In addition, it prevents oxidative addition by **9** to a putative **14b**, too

much crowded. Thus, the decomposition of **12b** leads directly and efficiently to **13** and black Pd.

3.2.b. Transmetalation to [Pd(Rf)I(dppf)] (3b) in THF.

The reaction of [Pd(Rf)I(dppf)] (**3b**) with PhC≡CSnBu₃ (**9**) at 313 K in THF follows a pathway presumably similar to **3a**. The evolution of **3b** is slow because the I⁻/**9** ligand exchange + transmetalation step is slow. In fact, intermediate [Pd(Rf)(C≡CPh)(dppf)] (**11b**) was not detected because its formation rate is slower than its coupling rate to [Pd(η²-PhC≡CRf)(dppf)] (**12b**) and **13** (Fig. 12). Although **12b** is an important early component of the mixture, eventually PhC≡CRf (**13**), released from slow decomposition of **12b**, becomes the main product. The increasing concentration of alkyne **13** (putative **14b** is not formed) is in this case the only responsible for the abnormally high deceleration of **3b** conversion.
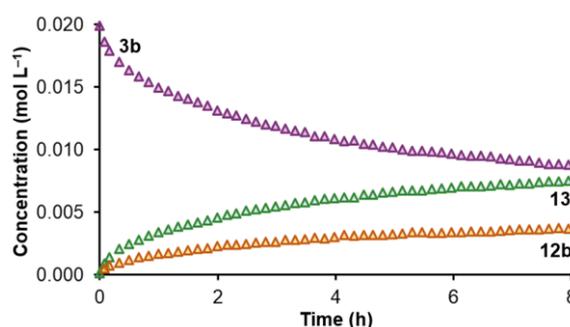
Fig. 12. ¹⁹F NMR monitoring of the reaction between [Pd(Rf)I(dppf)] (**3b**) and PhC≡CSnBu₃ (**9**) (Pd:Sn = 1:20) in THF at 313 K.

3.3.a. Transmetalation to [Pd(Rf)(OTf){PPh₂(bzN)}] (4c) in THF.

The behaviour of [Pd(Rf)(OTf){PPh₂(bzN)}] (**4c**) reacting with PhC≡CSnBu₃ (**9**) in THF is similar to the dppe complex **4a**, also in the non-observation of black Pd, although differences in the relative rates of the different steps (different $\Delta\Delta G^\ddagger$ for the steps with PPh₂(bzN) *vs.* the steps with dppe) produce dramatic graphical modifications in the profiles observed (Fig. 13).
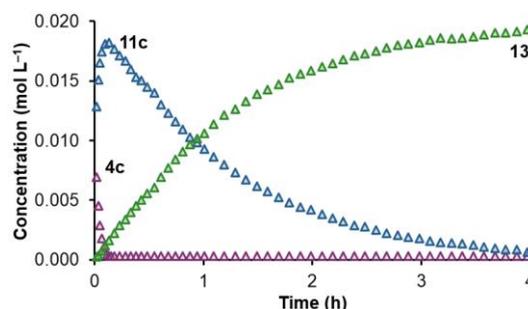
Fig. 13. ¹⁹F NMR monitoring of the reaction between [Pd(Rf)(OTf){PPh₂(bzN)}] (**4c**) and PhC≡CSnBu₃ (**9**) (Pd:Sn = 1:20) in THF at 313 K.

The transmetalation step on **4c** giving rise to intermediate [Pd(Rf)(C≡CPh){PPh₂(bzN)}] (**11c**) is only somewhat slower than for **4a**, but the C–C coupling to form **12c**, and the subsequent oxidative addition of **9** to give **14c**, are considerably faster. The reaction is complete after 4 hours (*vs.* 16 hours for **4a**) and only the final products **13** (in the ¹⁹F NMR monitoring) and **14c** (in the ³¹P NMR spectrum) can be observed at 313 K. A cis-P,Sn configuration of the

phosphine and the stannyl groups is safely assigned for **14c**, based on the small $^2J_{PSn}$ coupling constants ($^2J_P{}^{117}{}_{Sn}$ and $^2J_P{}^{119}{}_{Sn} \approx 15$ Hz, see Fig. ESI 9).[36]

3.3.b. Transmetalation to [Pd(Rf)I{PPh₂(bzN)}] (3c) in THF.

For the reaction of [Pd(Rf)I{PPh₂(bzN)}] (**3c**) with PhC≡CSnBu₃ (**9**) in THF at 313 K, the profile of the reaction obtained by ^{19}F NMR shows only the disappearance of **3c** and the formation of **13** (Fig. 14). The fast rates following the slow transmetalation prevent any observation in the ^{19}F monitoring other than the formation of **13**.
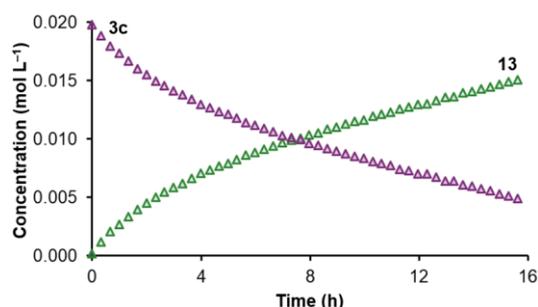

Fig. 14. ^{19}F NMR monitoring of the reaction between [Pd(Rf)I{PPh₂(bzN)}] (**3c**) and PhC≡CSnBu₃ (**9**) (Pd:Sn = 1:20) in THF at 313 K.

4. Analysis of the transmetalation mechanism.

Mechanistic proposals requiring dissociation of one coordinating end of the chelates can be discarded for the diphosphine complexes because this is a high energy process, and also for the PPh₂(bzN) complexes since they behave similarly. The most reasonable mechanisms for all the cases studied here are open mechanisms, with transmetalations initiated by S$_N$2 associative ligand substitution *via* pentacoordinate intermediates, with retention of the coordination site (Scheme 5).
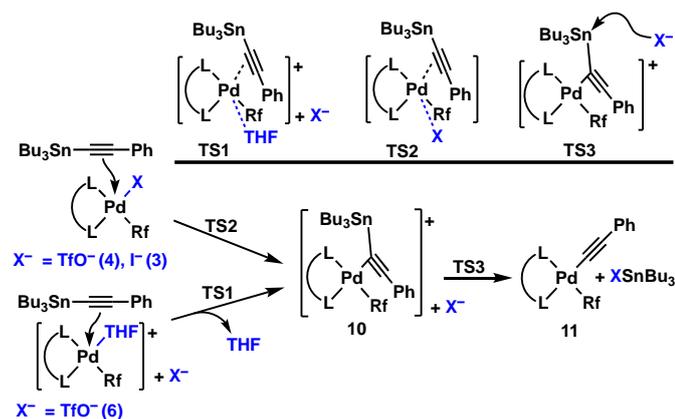
Scheme 5. Proposed mechanism for the transmetalation reaction, starting on **3**, **4**, or **6**. Above, the transition states of the initial ligand substitution (TS1 or TS2), and the subsequent transmetalation (TS3).

The cases of cationic (**6**) or neutral (**4** and **3**) starting complexes are represented. In just one step they all lead to the same intermediate **10**(X). As we have seen in our kinetic studies, this ligand substitution is difficult for **3**, and very easy for **4** or **6**. Finally, S$_N$2 attack of X⁻ (X = I, OTf) to the electrophilic Sn centre leads to concerted evolution to **11** and XSnBu₃. Support for this proposal is multiple: *i)* the alkynyl triple bond is a better donor than the vinyl double bond, which was

reported to follow this kind of pathway by DFT calculations,[29] hence alkynyl makes the ligand substitution easier; *ii)* as discussed for Fig. 6, the involvement of **BD(1) C1–Sn** as donor NBO in intermediates **10⁺** enhances the electrophilicity of Sn and facilitates the mechanism proposed in Scheme 5 for conversion to **11**. The transmetalations are extremely fast with coordinated OTf or coordinated THF starting complexes, because they make Pd a more electrophilic centre, and because they are better leaving ligands than iodide. Overall this makes the reductive elimination to be rate limiting for them. The unequal capability for the ligands used to promote C–C bond formation is clear, revealing a sequence dppf >> PPh₂(bzN) > dppe according to the different times needed to achieve total conversion of the coupling products into PhC≡CSnBu₃ (less than 30 min at 295 K for dppf, 4 and 16 hours at 313 K for PPh₂(bzN) and dppe respectively). For the iodo derivatives the transmetalation turns out to be always the *rds*.

Conclusions

The study of the speciation of some [Pd(Rf)X(P-L)] complexes with chelating ligands and its subsequent reactivity with PhC≡CSnBu₃ in the absence of an electrophile as oxidant, offers a frustrated Stille process that allows to uncover aspects that would remain hidden in a running cycle.

The speciation studies show that some neutral starting complexes can be immediately transformed in cationic complexes in an appropriate solvent, which will change its reactivity as has been discussed in previous studies.[3] Particularly interesting, this change of Pd species is possible not only from starting complexes with weak anionic ligands (X⁻ = TfO⁻) but also for those with halides (X⁻ = I⁻, Cl⁻) if a good solvating solvent is chosen in order to compensate for dissociation energy.

All the reactions in THF start with ligand substitution of X⁻ or coordinated THF by the entering alkynyl triple bond, *via* open alkynyl transmetalation. This ligand substitution step is fast for the easy leaving TfO⁻ or THF, and considerably slower for I⁻.

In the absence of the natural oxidative addition reagent that restarts the cycle (RfI in this case), the evolution of the process can be monitored, observing very different influences of X and the ligand on the evolution and rates of the ligand substitution, transmetalation, and reductive elimination processes. The formation of cationic species facilitates the ligand substitution and, consequently the transmetalation, due to increased electrophilicity of the Pd centre. In THF, the stronger ligand I⁻ always makes the evolution of the system slower.

An interesting effect of the chelating ligand is observed for dppf. Because it is a wide bite ligand, it promotes fast coupling to PhC≡CRf of the transmetalated intermediate and hinders oxidative addition of the Pd⁰ byproduct by PhC≡CSnBu₃. This leads to early formation of black Pd and PhC≡CRf as the products of the reaction. For the other ligands, in the circumstances of absence of RfI, the alkynylstannane PhC≡CSnBu₃, which is in addition the alkynyl-transmetalating nucleophile, is additionally able to act as oxidant at the end of the reaction, preventing for long time the formation of black Pd. The reaction products are PhC≡CRf and [Pd(C≡CPh)(SnBu₃){PPh₂(bzN)}] or [Pd(C≡CPh)(SnBu₃)(dppe)].

This work shows that carrying out the study of successive catalytic steps in an *on-purpose* frustrated cycle is a useful strategy to understand problems associated to catalytic synthesis. However, tin derivatives are slow transmetalating reagents, and similar studies

with faster nucleophiles may require monitoring at lower temperatures.

Conflicts of Interest

There are no conflicts to declare.

Notes and references

‡ Dedicated to so many people working in the health services worldwide, who, at the time this manuscript is being submitted for publication, continue bravely fighting to control the COVID-19 pandemic, too often with only limited media and risk for their own lives.

1 T. J. Colacot, *New Trends in Cross-Coupling. Theory and Applications*, Royal Society in Chemistry, Cambridge, UK, 2015.

2 For a recent review for application of the Stille reaction in the synthesis of natural products see: M. M. Heravi and L. Mohammadkhani, *J. Organomet. Chem.*, 2018, **869**, 106–200.

3 P. Espinet and A. M. Echavarren, *Angew. Chem., Int. Ed.,* 2004, **43**, 4704–4734.

4 C. Cordovilla, C. Bartolomé, J. M. Martínez-Ilarduya and P. Espinet, *ACS Catal.,* 2015, **5**, 3040–3053.

5 A. L. Casado and P. Espinet, *J. Am. Chem. Soc.*, 1998, **120**, 8978–8985.

6 A. L. Casado, P. Espinet and A. M. Gallego, *J. Am. Chem. Soc.*, 2000, **122**, 11771–11782.

7 For a recent review about solvent effects in Pd chemistry see: J. Sherwood, J. H. Clark, I. J. S. Fairlamb and J. M. Slattery, *Green Chem.*, 2019, **21**, 2164–2213.

8 A. L. Casado, P. Espinet, A. M. Gallego and J. M. Martínez-Ilarduya, *Chem. Commun.*, 2001, 339–340.

9 A. Fihri, P. Meunier and J.-C. Hierso, *Coord. Chem. Rev.*, 2007, **251**, 2017–2055.

10 (a) Y. Y. Belosludtsev, R. K. Bhatt and J. R. Falck, *Tetrahedron Lett.*, 1995, **36**, 5881–5882; (b) A. S. Gajare, R. S. Jensen, K. Toyota, M. Yoshifuji and F. Ozawa, *Synlett*, 2005, 144–148; (c) C. M. Crawforth, S. Burling, I. J. S. Fairlamb, A. R. Kapdi, R. J. K. Taylor and A. C. Whitwood, *Tetrahedron*, 2005, **61**, 9736–9751.

11 J. Mateos, E. Rivera-Chao and M. Fañanás-Mastral, *ACS Catal.*, **2017**, *7*, 5340–5344.

12 E. Shirakawa, H. Yoshida and T. Hiyama, *Tetrahedron Lett.*, 1997, **38**, 5177–5180.

13 E. Shirakawa and T. Hiyama, *J. Organomet. Chem.*, 1999, **576**, 169–178.

14 M. H. Pérez-Temprano, A. M. Gallego, J. A. Casares, and P. Espinet, *Organometallics*, 2011, **30**, 611–617.

15 An interesting kinetic study of the oxidative additionstep, in the context of the catalytic cycle, is available, but it does not provide much information on the intricate transmetalation and reductive elimination steps: B. Crociani, S. Antonaroli, L. Canovese, P. Uguagliati, and F. Visentin, *Eur. J. Inorg. Chem.* 2004, 732–742.

16 P. Espinet, J. M. Martínez-Ilarduya, C. Pérez-Briso, A. L. Casado and M. A. Alonso, *J. Organomet. Chem.*, 1998, **551**, 9–20.

17 To see bite angle values: M.-N. Birkholz, Z. Freixa and P. W. N. M. van Leeuwen, *Chem. Soc. Rev*, 2009, **38**, 1099–1118.

18 For X-ray crystal structures with bridging dppf see: G. Bandoli and A. Dolmella, *Coord. Chem. Rev*., 2000, **209**, 161–196.

19 R. G. Pearson, *Inorg. Chem.*, 1973, **12**, 712–713.

20 (a) J. A. Casares, P. Espinet, J. M. Martínez-Ilarduya and Y.-S. Lin, *Organometallics*, 1997, **16**, 770–779; (b) J. A. Casares,

S. Coco, P. Espinet and Y.-S. Lin, *Organometallics*, 1995, **14**, 3058–3067.

21 I. R. Butler, W. R. Cullen, T.-J. Kim, S. J. Rettig and J. Trotter, *Organometallics*, 1985, **4**, 972–980.

22 In general, one might expect the ionic complex side (two components) to be entropically favoured at higher temperature vs. the neutral complex one (one component), but the opposite is observed, according to the negative value of entropy. This indicates that solvation of the ionic complex is a major contribution that compensates the formation of two particles.

23 For NMP conductivity values see: A. K. Banerjee, A. J. Layton, R. S. Nyholm and M. R. Truter, *J. Chem. Soc. (A)*, 1969, 2536–2543.

24 The formation of *cis*-[Pd(Rf)(solv)$_2${PPh$_2$(bzN)-κ^1-P}] should produce F^o equivalence.

25 For a recent example of the Stille reaction using alkynylstannanes see: A. S. Levashov, D. S. Buryi, O. V. Goncharova, V. V. Konshin, V. V. Dotsenko and A. A. Andreev, *New J. Chem.*, 2017, **41**, 2910–2918.

26 S. Hoops, S. Sahle, R. Gauges, C. Lee, J. Pahle, N. Simus, M. Singhal, L. Xu, P. Mendes and U. Kummer, *Bioinformatics*, 2006, **22**, 3067–3074.

27 For cationic Pd^{II} complexes with coordinated alkynes (particularly Me$_3$Si–C≡C–SiMe$_3$) see A. M. LaPointe and M. Brookhart, *Organometallics*, 1998, **17**, 1530–1537.

28 This proposal is supported by several observations: the F^p signal appears at low-field, which is characteristic of cationic compounds; ^{31}P{^{1}H} NMR shows that the two P atoms are inequivalent; besides, this compound evolves to the transmetalation compound **11a**.

29 A. Nova, G. Ujaque, F. Maseras, A. Lledós and P. Espinet, *J. Am. Chem. Soc.*, 2006, **128**, 14571–14578.

30 C. Amatore, G. Broeker, A. Jutand and F. Khalil, *J. Am Chem. Soc.*, 1997, **119**, 5176–5185.

31 An excess of 10 eq. of **9** per palladium was added to a solution of [Pd(dppe)(dba)] in THF at room temperature. After 5 min. the ^{31}P{^{1}H} NMR shows the formation of **14a**.

32 H. S. Huh, Y. K. Lee and S. W. Lee, *J. Mol. Struct.*, 2006, **789**, 209–219.

33 E. G. Hope, R. D. W. Kemmitt and A. M. Stuart, *J. Chem. Soc., Dalton Trans.,* 1998, 3765–3770.

34 B. Cordero, V. Gómez, A. E. Platero-Prats, M. Revés, J. Echeverría, E. Cremades, F. Barragán and S. Alvarez, *Dalton Trans.*, 2008, 2832–2838.

35 M. N. Peñas-Defrutos, C. Bartolomé, M. García-Melchor and P. Espinet, *Angew. Chem. Int. Ed.*, 2019, **58**, 3501–3505.

36 With these small coupling constants the ^{117}Sn and ^{119}Sn satellites cannot be observed separately.